PHYSICAL REVIEW A VOLUME 57, NUMBER 3 MARCH 1998

Angle-resolved two-dimensional mapping of electron emission following Cl $2p$ excitations in the HCl molecule

E. Kukk,[1,2] A. Wills,[1] N. Berrah,[1] B. Langer,[3] J. D. Bozek,[2] O. Nayadin,[1] M. Alsherhi,[1] A. Farhat,[1] and D. Cubaynes[4]

[1]*Department of Physics, Western Michigan University, Kalamazoo, Michigan 49008-5151*

[2]*Lawrence Berkeley National Laboratory, University of California, Berkeley, California 94720*

[3]*Fritz-Haber-Institut der Max-Planck-Gesellschaft, Faradayweg 4-6, D-14195 Berlin, Germany*

[4]*Laboratoire de Spectroscopie Atomique et Ionique, URA 775, CNRS, Université Paris–Sud, 91405 Orsay, France*

(Received 17 November 1997)

Angle-resolved Auger and valence photoelectron spectra of HCl were measured over a 14-eV-wide photon-energy range across the Cl $2p$ ionization thresholds. Auger decay spectra of dissociative core-excited states were observed to change with photon energy, reflecting a change in the rate of dissociation. Auger electron spectra at the first Rydberg states were analyzed and the evolution of the resonant Auger to the normal Auger decay distorted by postcollision interaction was examined. Valence photoionization channels were shown to resonate strongly at the photon energies of the core-to-Rydberg excitations. Angular distributions of the photo- and Auger electron lines were derived; strong fluctuations of the β values of the 2π photoline were observed at some Rydberg resonances. Anisotropy of the Auger decay at the σ^* and Rydberg excitations was found to be different, with the latter showing uniformly negative β values. [S1050-2947(98)50203-X]

PACS number(s): 32.80.Hd, 33.80.Gj, 33.80.Eh

Inner-shell processes in small molecules have been studied with growing interest during recent years. Rapid improvements in experimental techniques have revealed new details in Auger and photoelectron spectra, such as anisotropy of electron emission [1–6], molecular field splitting [7], and postcollision interaction [8]. However, these studies have been performed at only a few selected photon energies. The aim of this Rapid Communication is to present a complete angle-resolved two-dimensional experimental picture of electron emission from a diatomic molecule over the pre-edge structure and into the continuum of a core ionization threshold. This extensive set of data illustrates many phenomena associated with core excitation or ionization.

We have studied the electron emission from HCl following photoexcitation or ionization of the Cl $2p$ core levels using highly efficient time-of-flight (TOF) spectrometers. This technique coupled with a third-generation synchrotron radiation source and advanced data aquisition software allowed us to record two-dimensional (2D) electron emission data sets (the representation is described in Ref. [9]) over a 14-eV-wide photon-energy range in a kinetic-energy window covering the majority of the ejected electrons. The resulting 2D spectra illustrate the evolution of the electron emission processes as the photon energy is scanned toward and across the Cl $2p$ ionization thresholds. Angular distributions were obtained by recording the 2D data sets at four angles.

The experiments were carried out at the undulator beamline 9.0.1 at the Advanced Light Source synchrotron radiation facility. The photon beam intersected an effusive beam of HCl at the foci of two time-of-flight spectrometers mounted 144.7° apart in the plane perpendicular to the direction of the photon beam propagation [10]. Electron TOF spectra were measured simultaneously at 0° and 54.7° relative to the polarization plane of the incident radiation and again at 90° and 35.3° after rotating the chamber. A 167-V retarding voltage was used to disperse the flight times of the energetic electrons and thus improve the energy resolution. Calibration spectra of the Ne $2s$ and $2p$ photoelectron lines were used to obtain the scaling factors for the time-to-energy conversion [11]. The photon energy was stepped by 20 meV between successive electron TOF spectra to build up the 2D data set. The photon-energy resolution was set to 75 meV for this experiment.

The absorption spectrum of HCl around the Cl $2p$ ionization threshold [12] can be divided into three regions: (i) excitation to the antibonding σ^* orbital ($2p \rightarrow \sigma^*$), (ii) excitation to the Rydberg orbitals ($2p \rightarrow nl$), and (iii) ionization into the continuum ($2p \rightarrow \epsilon l$). These three regions are indicated on the total electron yield curve along the right side of Fig. 1. The 2D electron emission map, shown in the main panel of Fig. 1, was obtained at an angle of 90° relative to the polarization plane. In this map, the intensity of the electron signal is represented as different shades of gray. Electrons emitted with the same kinetic energy at different photon energies are aligned vertically in the 2D map. Those emitted with constant binding energy form diagonal lines across the map. The features in the different regions of the 2D map are discussed in detail below.

Broad bands in the total electron yield between 199.0 and 203.5 eV correspond to excitation of the $2p$ electrons to the first unoccupied molecular orbital, σ^*. When occupied, this antibonding orbital causes the core-excited molecule to dissociate. The dissociation, $HCl^*(2p^5\sigma^*) \rightarrow H(1s) + Cl^*(2p^5 3p^6)$, produces neutral hydrogen and core-excited chlorine atoms and proceeds on a time scale ($\approx 10^{-14}$ s) that competes with the Auger decay of the core hole [13,14]. The light hydrogen atom moves quickly away from the Cl atom, so that a large part of the Auger decay occurs in the atomic chlorine as $2p^5 3p^6 \rightarrow 3p^4$ transitions, seen as intense vertical lines in the 2D map at the photon energies of the $2p \rightarrow \sigma^*$ excitation. These sharp atomic lines have pronounced tails at their low-kinetic-energy side arising

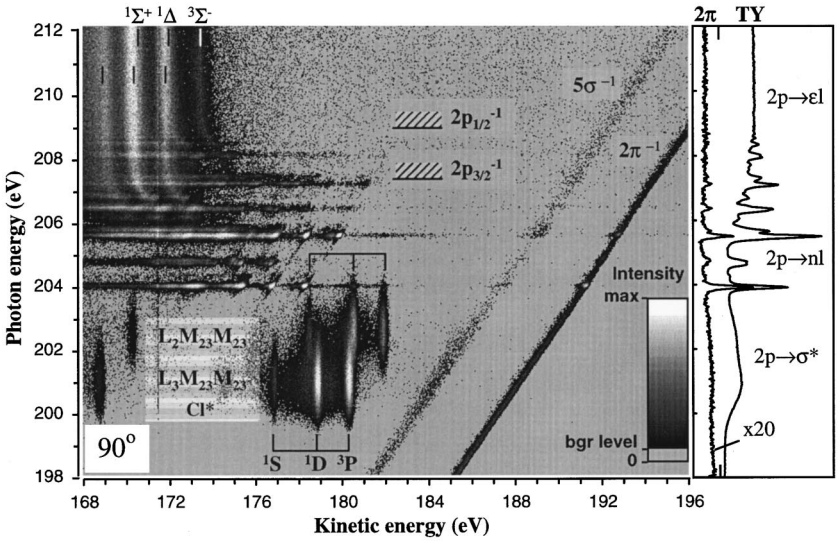

FIG. 1. Two-dimensional (2D) map of electron emission from the HCl molecule across the Cl $2p$ ionization threshold, taken at 90° relative to the polarization plane. The total electron and partial 2π photoelectron yields are shown on the right.

from Auger transitions in the molecular environment prior to the complete dissociation. These tails form a ''molecular background'' to the atomic Auger spectrum [14].

As the photon energy is increased across the breadth of the σ^* band, HCl molecules with decreasing internuclear separation are selected due to the projection of the ground-state population onto the dissociative potential-energy curve. This shift may influence the time scale of the early stage of the dissociation, which should be reflected in the balance between the molecular background and the sharp atomic peaks in the Auger spectra. In order to investigate this possibility, the intensities of one atomic line and its associated background were monitored as a function of photon energy; they are compared in Fig. 2. The $2p_{1/2}^{-1}3p^6 \rightarrow 3p^4(^3P)$ atomic line at a kinetic energy of 182.0 eV was selected, since it is well separated from neighboring peaks. The molecular tail of this line is assigned to transitions to the $^4\Sigma^-$, $^2\Sigma^-$ and $^4\Pi$ states of HCl^+ [14]. The distinction between the atomic and molecular regions is somewhat arbitrary. Here, we represent the latter by choosing the part of the spectrum between the ^1D and ^3P lines, from 180.8 to 181.8 eV. The solid line in Fig. 2 is a Gaussian fit to the $2p_{1/2} \rightarrow \sigma^*$ total yield peak. The molecular part of the Auger spectrum dominates at photon energies well below the absorption peak maximum. With increasing photon energy, the internuclear distance at which the excitation can take place shifts to smaller values, where the energy of the core excited state is higher. Here the atomic peak gains intensity over the molecular background, inferring a higher dissociation rate. This effect can be related to the slope of the potential-energy curve of the excited state. At lower photon energies the molecular ground state is projected onto the lower part of the potential-energy curve of the $2p_{1/2}^{-1}\sigma^*$ state, where the curve is less steep. The dissociation rate and Auger line shape depend on the slope of the potential-energy curve at the point of excitation [14]: a smaller slope leads to a smaller initial acceleration of the fragments and consequently to a lower dissociation rate and *vice versa*. At the photon energies well above the peak maximum, the spectra are strongly affected by the overlap with the $2p_{3/2}^{-1}4s$ resonance and at smaller emission angles also by 4σ photoelectron satellite lines that start to cross this kinetic-energy region. We do not see conclusive evidence that the molecular background is again enhanced at the high-energy side of the resonance due to the shortening of the duration time of the resonant scattering process at larger detunings, as proposed in Ref. [15].

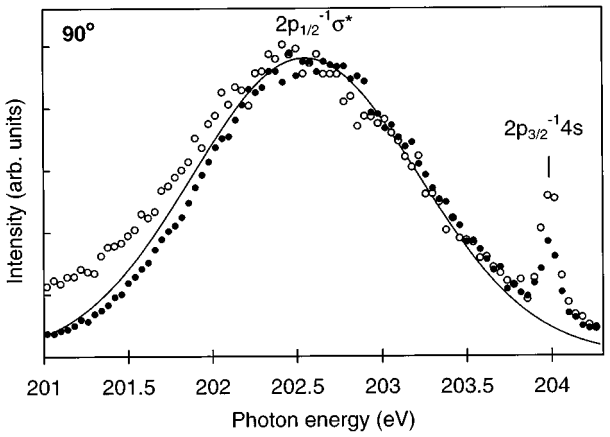

FIG. 2. Photon-energy dependency of the $L_2-M_{2,3}M_{2,3}(^3P)$ chlorine atomic Auger line (filled circles) and its molecular tail (open circles). Gaussian fit to the $2p_{1/2} \rightarrow \sigma^*$ absorption peak is shown by a solid line.

A quite different pattern of Auger decay can be seen in the region of the sharp core-to-Rydberg excitations starting at 204.0-eV photon energy. The spectral structures here arise from molecular Auger decay and are assigned within the simplest spectator model as the $2p^{-1}nl \rightarrow (4\sigma 5\sigma 2\pi)^{-2}n'l'$ transitions, where nl and $n'l'$ describe the Rydberg electron in the Auger initial and final state, respectively [16]. This region of the 2D map is expanded in Fig. 3 and shown on a binding-energy scale, where transitions to the same final ionic states are aligned vertically.

The tail of the $2p_{1/2}^{-1}\sigma^*$ resonance overlaps with the first Rydberg resonance $2p_{3/2}^{-1}4s$ at 204.0 eV (see Figs. 1 and 2). The intensity of the Auger lines from the decay of the dissociating $2p_{1/2}^{-1}\sigma^*$ state shows a sharp increase at the $2p_{3/2}^{-1}4s$ resonance (Fig. 2). At the magic angle, these Auger lines account for about 6% of the total Auger intensity at this photon energy. About half of their intensity comes from the

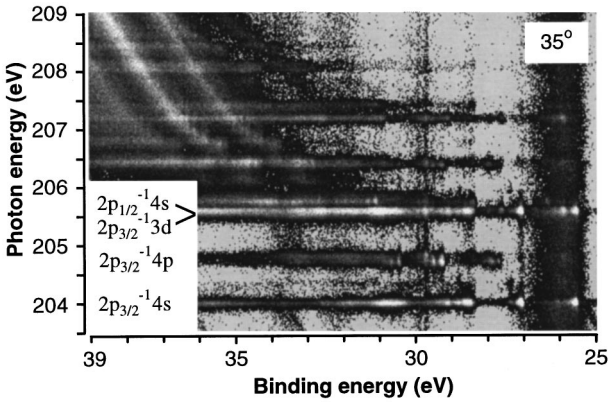

FIG. 3. 2D map of Auger electron emission at the Rydberg resonances measured at 35.3°.

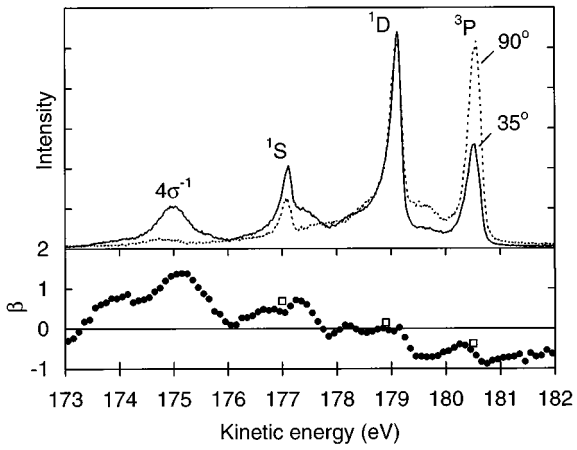

FIG. 4. Electron-energy spectra, extracted at the $2p_{3/2}^{-1}\sigma^*$ resonance. Lower panel shows the angular parameter β. Rectangles are the values from Ref. [4].

overlap with the Gaussian-shaped tail of the $2p_{1/2}^{-1}\sigma^*$ resonance. The remainder is resonant enhancement, indicating the possibility of predissociation on the first Rydberg resonance. The transition from the bound $2p_{3/2}^{-1}4s$ to dissociative $2p_{1/2}^{-1}\sigma^*$ potential-energy curve must involve some interaction between the two spin-orbit components of the $2p$ orbital. Detailed calculations of these potential-energy curves are needed to investigate this effect further.

The next Rydberg resonance, $2p_{3/2}^{-1}4p$, is broader than the others in the absorption spectrum, apparently consisting of two overlapping peaks of equal intensity, separated by about 100 meV [12,16]. The 2D maps exhibit a unique pattern for this resonance, suggesting that it is split into two levels that have different Auger electron spectra. On the lower-energy side of the resonance, the Auger intensity is concentrated in the binding-energy region of the $2\pi^{-2}n'l'$ final states, whereas the higher-energy side tends to populate the higher-binding-energy $5\sigma^{-1}2\pi^{-1}n'l'$ and $5\sigma^{-2}n'l'$ states. If the two states underlying this resonance correspond to the molecular field splitting of the $2p_{3/2}$ core orbital into $2p_{3/2,1/2}$ and $2p_{3/2,3/2}$ components (using the nl_{j,m_j} notation), then the different population of Auger final states can be explained by different orientations of the core hole. In the lower-energy state, $2p_{3/2,3/2}^{-1}4p$, the core hole has a purely π character [17] and therefore exhibits a large overlap with the valence π orbital in the Auger matrix elements, whereas the $2p_{3/2,1/2}$ hole has a mostly σ character and overlaps more with the 5σ orbital.

The intensity of the Auger spectra of the higher Rydberg states gradually shifts towards higher binding energies due to the weakening of the influence of the spectator electron and higher shake-up probability. Finally, the $2\pi^{-2}n'l'$ resonant Auger lines merge into the $2\pi^{-2}(^3\Sigma^-,{}^1\Delta,{}^1\Sigma^+)$ normal Auger lines. There is no sudden change in the Auger decay pattern at the $2p$ ionization thresholds (marked in Fig. 1, from Ref. [12]). Rather there is a smooth evolution from the spectator to normal Auger spectra through a strong postcollision interaction (PCI). The energy shift of the normal Auger lines, caused by the PCI between the outgoing slow $2p$ photoelectron and Auger electron, can be seen through the threshold down to the Rydberg states. The shift below the threshold is caused by the screening effect of the bound, core-excited electron. This evolution is best described by the nonradiative resonant Raman-scattering theory [18]. No marked difference can be observed between the energy shifts of the Auger lines in the spectra taken at different angles. The $2p_{1/2}^{-1}\rightarrow 2\pi^{-2}(^3\Sigma^-)$ normal Auger line at the $2p_{1/2}$ threshold ($h\nu=209.03$ eV) is shifted by about 140 meV with respect to its position 3 eV above the threshold, in both the 35° and 90° spectra.

The 2π photoelectron yield (see Fig. 1) exhibits a clear enhancement at some of the Cl $2p$ Rydberg resonances. The relative increase is strongest in the spectrum measured at 90°, where the photoline intensity increases about 4 times at the $2p_{3/2}^{-1}4s$ resonance. After subtracting the constant direct ionization contribution, the intensity of the resonant channel is about 30% of the strongest spectator Auger transition to the $2\pi^{-2}(^1\Delta)n'l'$ state (at $E_b=27.3$ eV) at both 90° and the magic angle. Another strong resonant enhancement of the 2π photoline is seen at 205.6-eV photon energy. Based on the peak position, we attribute this increase in intensity to the $2p_{1/2}^{-1}4s$, rather than $2p_{3/2}^{-1}3d$ Rydberg resonance. The 5σ photoelectron line is also enhanced at the $2p_{3/2}^{-1}4s$ resonance, though to a lesser extent. The largest increase, 1.9 times, is again seen at 90°. The intensities of the 2π and 5σ photolines do not change dramatically at the other Rydberg states and thus the resonance behavior seems to be mainly characteristic of the $2p^{-1}4s$ states. The profiles of the resonances in the photoelectron yield are symmetric, contrary to the strongly asymmetric profiles that would be expected from the interference between the direct and resonant ionization channels of comparable amplitudes. The strong resonant contribution to the valence photoionization is surprising in light of recent results for other diatomic molecules like CO, for which an almost total absence of any participator contribution in the decay of Rydberg states has been noted [6]. The resonant behavior of the photolines could be a result of either participator decay of the core-excited state or Auger final-state configuration mixing. In the latter case the $2\pi^{-1}(^2\Pi)$ ionic state would, e.g., acquire some character of the higher $^2\Pi$ states that are directly accessible via spectator Auger transitions, like $5\sigma^{-1}2\pi^{-1}4s(^2\Pi)$.

Anisotropy in the electron emission is described by a single parameter β, which in the case of direct ionization derives from the shape of the initial- and final-state wave functions of the photoelectron. The β parameter for the Au-

ger electrons is given as a product of a molecular alignment parameter and an intrinsic anisotropy parameter for the Auger decay [19]. At first, the β values of the 2π and 5σ photolines were determined at resonant photon energies using their branching ratios with some Auger lines that exhibit opposite angular asymmetry from the spectra measured at three angles. The 2π photoline intensity at these resonances together with its obtained β value were then used for intensity normalization of the 2D maps so that all other β values could be determined directly by comparing spectra measured at two angles.

The β parameters for the 2π and 5σ photolines are considered first. They have equal values of 1.6(2) below the Rydberg resonances. At the first Rydberg resonance, the β value of the 2π line drops to 0.90(10), whereas the β of the 5σ line shows no change. At the next strong (overlapping) resonances $2p_{3/2}^{-1}3d$ and $2p_{1/2}^{-1}4s$, the value of β for the 2π line drops again to 1.15(10). These changes in the value of β also indicate that a resonant valence ionization channel becomes available.

Auger electron spectra at 35° and 90° relative to the polarization plane, measured at the $2p_{3/2}^{-1}\sigma^*$ resonance, are shown in Fig. 4 together with derived β values. The β values of the Auger lines vary between -0.7 and 0.7. Strongly positive β values near 175 eV are assigned to the direct 4σ ionization. Our results are in good agreement with those of Becker and Menzel [4], who determined the β parameters for the three atomic lines only. The molecular background also shows large variations of the angular parameter, which, when combined with theoretical calculations, should prove useful for refining the assignment of the spectrum.

The β values for the Auger lines show a markedly different behavior at the Rydberg resonances. At the $2p_{3/2}^{-1}4s$ resonance, all Auger lines have negative β values. The $2\pi^{-2}(^1\Delta)4s$ line at $E_b=27.3$ eV has the largest anisotropy with $\beta=-0.7(2)$, which infers that the molecule is strongly aligned after the $2p_{3/2}\rightarrow 4s$ excitation. We also observed negative β values at the overlapping $2p_{3/2}^{-1}3d$, $2p_{1/2}^{-1}4s$ resonances. All of the molecular Auger lines have similar β values, and for the the normal Auger lines β parameters are equal within the error limits, since there is no change in the branching ratios of the Auger lines at different angles.

In conclusion, the 2D electron emission mapping technique has been shown to be a valuable tool for investigating various characteristics over large kinetic- and photon-energy ranges. In particular, the following effects have been observed: (i) a photon-energy-dependent dissociation rate of the core-excited molecule as reflected in the Auger electron spectra; (ii) very strong resonant behavior of the 2π photoelectron yield at $2p^{-1}4s$ Rydberg resonances, observed both in the intensity and angular distributions; (iii) a link of the first Rydberg state to the $2p_{1/2}^{-1}\sigma^*$ state, leading to an increased dissociation probability; and (iv) different Auger decay patterns of the split $2p_{3/2}^{-1}4p$ resonance levels, possibly associated with core-hole orientation. In addition, the angular distributions of the Auger electrons at the σ^* and Rydberg excitations were found to be different, with the latter showing uniformly negative β values.

This work was supported, under Contract No. DE-FG02-95ER14299, by the U.S. Department of Energy, Office of Basic Energy Science, Division of Chemical Sciences.

[1] U. Becker, R. Hölzel, H. G. Kerkhoff, B. Langer, D. Szostak, and R. Wehlitz, Phys. Rev. Lett. **56**, 1455 (1986).
[2] O. Hemmers, F. Heiser, J. Eiben, R. Wehlitz, and U. Becker, Phys. Rev. Lett. **71**, 987 (1993).
[3] U. Hergerhahn and U. Becker, J. Electron Spectrosc. Relat. Phenom. **72**, 243 (1995).
[4] U. Becker and A. Menzel, Nucl. Instrum. Methods Phys. Res. B **99**, 68 (1995).
[5] A. Kivimäki, M. Neeb, B. Kempgens, H. M. Köppe, and A. M. Bradshaw, Phys. Rev. A **54**, 2137 (1996).
[6] S. Sundin, S. J. Osborne, A. Ausmees, O. Björneholm, S. L. Sorensen, A. Kikas, and S. Svensson, Phys. Rev. A **56**, 480 (1997).
[7] H. Aksela, E. Kukk, S. Aksela, O.-P. Sairanen, A. Kivimäki, E. Nõmmiste, A. Ausmees, S. J. Osborne, and S. Svensson, J. Phys. B **28**, 4259 (1995).
[8] M. Neeb, M. Biermann, and W. Eberhardt, J. Electron Spectrosc. Relat. Phenom. **69**, 239 (1994).
[9] A. A. Wills, D. Čubrić, M. Ukai, F. Currell, B. J. Goodwin, T. Reddish, and J. Comer, J. Phys. B **26**, 2601 (1993).
[10] B. Langer, N. Berrah, A. Farhat, O. Hemmers, and J. D. Bozek, Phys. Rev. A **53**, R1946 (1996).
[11] N. Berrah, B. Langer, J. D. Bozek, T. W. Gorczyca, O. Hemmers, D. W. Lindle, and O. Toader, J. Phys. B **29**, 1 (1996).
[12] D. A. Shaw, D. Cvejanović, G. C. King, and F. D. Read, J. Phys. B **17**, 1984 (1984).
[13] P. Morin and I. Nenner, Phys. Rev. Lett. **56**, 1913 (1986).
[14] E. Kukk, H. Aksela, O.-P. Sairanen, S. Aksela, A. Kivimäki, E. Nõmmiste, A. Ausmees, A. Kikas, S. J. Osborne, and S. Svensson, J. Chem. Phys. **104**, 4475 (1996).
[15] O. Björneholm, S. Sundin, S. Svensson, R. R. T. Marinho, A. Naves de Brito, F. Gel'mukhanov, and H. Ågren, Phys. Rev. Lett. **79**, 3150 (1997).
[16] E. Kukk, H. Aksela, O.-P. Sairanen, E. Nõmmiste, S. Aksela, S. J. Osborne, A. Ausmees, and S. Svensson, Phys. Rev. A **54**, 2121 (1996).
[17] K. Ellingsen, T. Saue, H. Aksela, and O. Gropen, Phys. Rev. A **55**, 2743 (1997).
[18] G. B. Armen, J. C. Levin, and I. A. Sellin, Phys. Rev. A **53**, 772 (1996).
[19] D. Dill, J. R. Swanson, S. Wallace, and J. L. Dehmer, Phys. Rev. Lett. **45**, 1393 (1980).